MULTISCALE MODEL. SIMUL.
Vol. 9, No. 1, pp. 258–281

AN EULERIAN SURFACE HOPPING METHOD FOR THE SCHRÖDINGER EQUATION WITH CONICAL CROSSINGS*

SHI JIN†, PENG QI†, AND ZHIWEN ZHANG‡

Abstract. In a nucleonic propagation through conical crossings of electronic energy levels, the codimension two conical crossings are the simplest energy level crossings, which affect the Born–Oppenheimer approximation in the zeroth order term. The purpose of this paper is to develop the surface hopping method for the Schrödinger equation with conical crossings in the Eulerian formulation. The approach is based on the semiclassical approximation governed by the Liouville equations, which are valid away from the conical crossing manifold. At the crossing manifold, electrons hop to another energy level with the probability determined by the Landau–Zener formula. This hopping mechanics is formulated as an interface condition, which is then built into the numerical flux for solving the underlying Liouville equation for each energy level. While a Lagrangian particle method requires the increase in time of the particle numbers, or a large number of statistical samples in a Monte Carlo setting, the advantage of an Eulerian method is that it relies on fixed number of partial differential equations with a uniform in time computational accuracy. We prove the positivity and l^1-stability and illustrate by several numerical examples the validity and accuracy of the proposed method.

Key words. surface hopping method, conical crossings, Liouville equation, Landau–Zener formula, interface condition, high resolution scheme

AMS subject classifications. 35Q40, 65M06

DOI. 10.1137/090774185

1. Introduction.

The quantum mechanical description of molecular dynamics is given by the time-dependent Schrödinger equation [27],

$$i\hbar\partial_t\Phi(t,\mathbf{x},\mathbf{y}) = H\Phi(t,\mathbf{x},\mathbf{y}), \tag{1}$$

$$\Phi(0,\mathbf{x},\mathbf{y}) = \Phi_0(\mathbf{x},\mathbf{y}). \tag{2}$$

Here $\hbar$ is the reduced Planck constant and $\Phi(t,\mathbf{x},\mathbf{y})$ is the total wave function. The vectors $\mathbf{x}\in\mathbb{R}^N$ and $\mathbf{y}\in\mathbb{R}^n$ denote the positions of N nuclei and n electrons, respectively. The molecular Hamiltonian operator H consists of two parts, the kinetic energy operator of the nuclei and the electronic Hamiltonian for fixed nucleonic configuration,

$$H = -\sum_{j=1}^{N}\frac{\hbar^2}{2M_j}\Delta_{x_j} + H_e(\mathbf{y},\mathbf{x})$$

with,

$$H_e(\mathbf{y},\mathbf{x}) = -\sum_{j=1}^{n}\frac{\hbar^2}{2m_j}\Delta_{y_j} + \sum_{j<k}\frac{1}{|y_j-y_k|} + \sum_{j<k}\frac{Z_jZ_k}{|x_j-x_k|} - \sum_{j=1}^{N}\sum_{k=1}^{n}\frac{Z_j}{|x_j-y_k|}.$$

*Received by the editors October 19, 2009; accepted for publication (in revised form) November 2, 2010; published electronically February 10, 2011. This work was partially supported by NSF grant DMS-0608720 and NSF FRG grant DMS-0757285.

http://www.siam.org/journals/mms/9-1/77418.html

†Department of Mathematics, University of Wisconsin, Madison, WI 53706 (jin@math.wisc.edu, pqi@math.wisc.edu). The first author was also supported by a Van Vleck Distinguished Research Prize and a Vilas Associate Award from the University of Wisconsin-Madison.

‡Department of Mathematics, Tsinghua University, Beijing, 100084, People's Republic of China (zhangzhiwen02@mails.tsinghua.edu.cn).

Here m_j denotes the mass of the j-th electron, and M_j, Z_j denote the mass and the charge of the j-th nucleus. The electronic Hamiltonian H_e consists of the kinetic energy of the electrons as well as the interelectronic repulsion potential, the internuclear repulsion potential, and the electronic-nuclear attraction potential.

The time-dependent Schrödinger equation (1) mathematically describes the fundamental physical behavior at the molecular scale. In principle, it is possible to describe all chemical systems by solving this equation. However, due to the high dimensionality of the molecular configuration space $\mathbb{R}^{N+n}$, numerical simulation of the Schrödinger equation (1) is a formidable challenge. For common molecules like carbon dioxide CO_2, which consists of 3 nuclei and 22 electrons, the full time-dependent Schrödinger equation is cursed by the high dimensionality of the molecular configuration space $\mathbb{R}^{75}$. The Born–Oppenheimer approximation is a commonly used approach in quantum chemistry to reduce the degrees of freedom.

This approximation was proposed in the early days of quantum mechanics by Born and Oppenheimer [3] and is still indispensable in quantum chemistry. It is built upon the mass discrepancy between the light electrons m and the heavy nuclei M in molecules. Due to the mass difference, the motions of the particles are in different time scales. The electrons move relatively fast, which are treated quantum mechanically, while the nuclei move relatively slowly, which can be considered as classical particles. This allows the wave function of a molecule to be split into its electronic and nuclear components.

Assume L is the typical length, T the typical time scale, Ω the typical mass scale, $m_j = m$, and $M_j = M\,\forall j$. Then one can nondimensionalize the Schrodinger equation (1) by introducing

$$\tilde{t} = \frac{t}{T}, \quad \tilde{\mathbf{x}} = \frac{\mathbf{x}}{L}, \quad \tilde{\mathbf{y}} = \frac{\mathbf{y}}{L}, \quad \tilde{m} = \frac{m}{\Omega}, \quad \tilde{M} = \frac{M}{\Omega},$$

$$\tilde{H}_e(\tilde{\mathbf{y}}, \tilde{\mathbf{x}}) = \frac{\tilde{m}T^2}{\Omega\hbar^2 L^2} H_e(\mathbf{y}, \mathbf{x}), \quad \tilde{\Phi}(\tilde{t}, \tilde{\mathbf{x}}, \tilde{\mathbf{y}}) = \Phi(t, \mathbf{x}, \mathbf{y}),$$

and obtain

$$i\delta\tilde{m}\partial_{\tilde{t}}\tilde{\Phi}(\tilde{t}, \tilde{\mathbf{x}}, \tilde{\mathbf{y}}) = -\sum_{j=1}^{N} \frac{\delta^2}{2}\frac{\tilde{m}}{\tilde{M}}\Delta_{\tilde{x}_j}\tilde{\Phi}(\tilde{t}, \tilde{\mathbf{x}}, \tilde{\mathbf{y}}) + \tilde{H}_e(\tilde{\mathbf{y}}, \tilde{\mathbf{x}})\tilde{\Phi}(\tilde{t}, \tilde{\mathbf{x}}, \tilde{\mathbf{y}}), \tag{3}$$

where $\delta = \frac{\hbar T}{\Omega L^2}$ is a dimensionless number. We let $\delta = 1$, $\hat{t} = \frac{\tilde{t}}{\sqrt{\tilde{m}\tilde{M}}}$, $\hat{\Phi}(\hat{t}, \tilde{\mathbf{x}}, \tilde{\mathbf{y}}) = \tilde{\Phi}(\tilde{t}, \tilde{\mathbf{x}}, \tilde{\mathbf{y}})$ and $\varepsilon = \sqrt{\frac{\tilde{m}}{\tilde{M}}}$; then (3) becomes

$$i\varepsilon\partial_{\hat{t}}\hat{\Phi}(\hat{t}, \tilde{\mathbf{x}}, \tilde{\mathbf{y}}) = -\sum_{j=1}^{N} \frac{\varepsilon^2}{2}\Delta_{\tilde{x}_j}\hat{\Phi}(\hat{t}, \tilde{\mathbf{x}}, \tilde{\mathbf{y}}) + \tilde{H}_e(\mathbf{y}, \mathbf{x})\hat{\Phi}(\hat{t}, \tilde{\mathbf{x}}, \tilde{\mathbf{y}}). \tag{4}$$

For convenience, in the following, we still use t, x, y, and H_e to stand for $\hat{t}$, $\tilde{x}$, $\tilde{y}$, and $\tilde{H}_e$, respectively. The time-dependent Schrödinger equation (1) then becomes

$$i\varepsilon\partial_t\Phi(t, \mathbf{x}, \mathbf{y}) = -\sum_{j=1}^{N} \frac{\varepsilon^2}{2}\Delta_{x_j}\Phi(t, \mathbf{x}, \mathbf{y}) + H_e(\mathbf{y}, \mathbf{x})\Phi(t, \mathbf{x}, \mathbf{y}). \tag{5}$$

In the Born–Oppenheimer approximation, one first solves the following time-independent *electronic* eigenvalue problems:

$$H_e(\mathbf{y},\mathbf{x})\varphi_k(\mathbf{y};\mathbf{x}) = E_k(\mathbf{x})\varphi_k(\mathbf{y};\mathbf{x}) \quad \forall \mathbf{x}\in\mathbb{R}^N,\ k=1,2,\dots. \tag{6}$$

Here one assumes that the spectrum of H_e is discrete with a complete set of orthonormal eigenfunctions $\{\varphi_k(\mathbf{y};\mathbf{x})\}$ called the *adiabatic* basis, over the electronic coordinates for every fixed nucleus coordinates; i.e.,

$$\int_{-\infty}^{\infty} \varphi_i^*(\mathbf{y};\mathbf{x})\varphi_j(\mathbf{y};\mathbf{x})d\mathbf{y} \equiv \langle \varphi_i(\mathbf{y};\mathbf{x})|\varphi_j(\mathbf{y};\mathbf{x})\rangle_{\mathbf{y}} = \delta_{ij},$$

where δ_{ij} is the Kronecker delta. The electronic energy eigenvalue $E_k(\mathbf{x})$, called the *potential energy surface*, depends on the positions of the nuclei. They can be obtained as a continuous function of $\mathbf{x}$ by varying $\mathbf{x}$ in small steps and repeatedly solving the eigenvalue problem (6).

Next the total wave function $\Phi(t,\mathbf{x},\mathbf{y})$ is expanded in terms of the eigenfunctions $\{\varphi_k\}$:

$$\Phi(t,\mathbf{x},\mathbf{y}) = \sum_k \chi_k(t,\mathbf{x})\varphi_k(\mathbf{y};\mathbf{x}). \tag{7}$$

Insert ansatz (7) into the time-dependent Schrödinger equation (5), multiply all the terms from the left by $\varphi_k^*(\mathbf{y};\mathbf{x})$, integrate with respect to $\mathbf{y}$, and then one obtains a set of coupled differential equations:

$$i\varepsilon\frac{\partial}{\partial t}\chi_k(t,\mathbf{x}) = \left[-\sum_{j=1}^N \frac{\varepsilon^2}{2}\Delta_{x_j} + E_k(\mathbf{x})\right]\chi_k(t,\mathbf{x}) + \sum_l C_{kl}\chi_l(t,\mathbf{x}), \tag{8}$$

where the coupling operator C_{kl} is defined by

$$C_{kl} \equiv \left\langle \varphi_k\right| -\sum_{j=1}^N \frac{\varepsilon^2}{2}\Delta_{x_j}\varphi_l\Big\rangle_{\mathbf{y}} - \sum_{j=1}^N \varepsilon^2\langle\varphi_k\big|\nabla_{x_j}\varphi_l\rangle_{\mathbf{y}}\cdot\nabla_{x_j}. \tag{9}$$

As long as the potential energy surfaces $\{E_k(\mathbf{x})\}$ are well separated, all the coupling operators C_{kl} are ignored since they describe the interactions between different energy levels. By ignoring C_{kl} in (8), one obtains a set of decoupled Schrödinger equations

$$i\varepsilon\frac{\partial}{\partial t}\chi_k(t,\mathbf{x}) = \left[-\sum_{j=1}^N \frac{\varepsilon^2}{2}\Delta_{x_j} + E_k(\mathbf{x})\right]\chi_k(t,\mathbf{x}), \quad (t,\mathbf{x})\in\mathbb{R}^+\times\mathbb{R}^N. \tag{10}$$

This means that the nuclear motion proceeds without the transitions between electronic states or energy surfaces. This is the essence of the *Born–Oppenheimer approximation* or *adiabatic approximation*. This kind of representation is called *adiabatic representation*.

In [34], Spohn and Teufel gave a rigorous analysis of the time-dependent Born–Oppenheimer approximation. They proved that the time-dependent Schrödinger equation (1) without energy level crossing can be approximated by the corresponding Born–Oppenheimer approximation solution with an error of order ε. For other rigorous mathematical study on Born–Oppenheimer approximation, see [5, 10, 12, 24].

When potential energy surfaces $E_k(\mathbf{x})$ approach each other, or even cross, the effect of the coupling operators C_{kl} in (8) becomes nonnegligible and the Born–Oppenheimer approximation breaks down. There will be *nonadiabatic transition* between the adjacent potential energy surfaces $E_k(\mathbf{x})$ and $E_l(\mathbf{x})$ [41]. This means that the nuclear motion proceeds with transitions between electronic states and the electronic wave functions can evolve from the reactant electronic configuration to the product electronic configuration, which makes the chemical bonds fission and the chemical reaction such as *charge transfer*, *photoisomerization*, or *photodissociation* happen. See [4] for more details.

To handle the transitions, one can alternatively consider the so-called *diabatic representation* [1]. Generally, let $U(\mathbf{x})$ denote a unitary transform matrix. We can see a unitary transformation in the vector space of electronic states does not change the total wave function (7),

$$\Phi = \sum_k \chi_k \varphi_k = \chi^+ \varphi = \chi^+ U^+ U \varphi = (U\chi)^+ (U\varphi) \equiv \tilde{\chi}^+ \tilde{\varphi},$$

where we denote the conjugate transpose of U by U^+, $\tilde{\varphi} = U\varphi$, and $\tilde{\chi} = U\chi$. If we can find the transformation $U(\mathbf{x})$ by which the the coupling operators C_{kl} vanish, the basis $\{\tilde{\varphi}_k(\mathbf{y};\mathbf{x})\}$ is called *diabatic* basis. Multiplying (10) from the left by U^+ gives

$$i\varepsilon \frac{\partial}{\partial t}\tilde{\chi}(t,\mathbf{x}) = \left[-\sum_{j=1}^{N} \frac{\varepsilon^2}{2}\Delta_{x_j} + V(\mathbf{x}) \right] \tilde{\chi}(t,\mathbf{x}), \quad (t,\mathbf{x}) \in \mathbb{R}^+ \times \mathbb{R}^N. \tag{11}$$

Here the potential $V(\mathbf{x}) = U^+ \mathtt{diag}(E_1(\mathbf{x}), E_2(\mathbf{x}), E_3(\mathbf{x}), \ldots) U$ is *not* a diagonal matrix any more. From (11) one can see that the coupling operators which have disappeared in (8) are reflected in the nondiagonal elements of the potential matrix $V(\mathbf{x})$. As U is a unitary matrix, all expectation values of observables remain the same under the diabatic transformation. However, it should be pointed out that the diabatic transformation can only be found for $1d$ problems by solving a differential equation. In other cases, it may not be possible to find a diabatic basis. Thus, people turn to find the so-called *quasi-diabatic* basis, which minimizes the coupling operators C_{kl}. The quasi-diabatic basis is commonly used and is efficient. In our paper, we assume in some basis, the coupling operators C_{kl} can be neglected. See [40] for more details about the diabatic representation.

For polyatomic molecules, which consist of more than two nuclei, the potential energy surface crossings can be very complicated. Hagedorn in [11] rigorously derived and classified 11 possible types of eigenvalue crossings of minimal multiplicity in molecular dynamics, and pointed out that the crossing manifold S can be of codimension 1, 2, 3, or 5 in the nucleonic configuration space.

One of the widely used approaches to simulate the nonadiabatic dynamics is the *surface hopping method*, first proposed by Tully and Preston in 1971 [36], and well developed since then [37, 38, 33]. The basic idea is to combine the classical transports of the system on individual potential energy surfaces with instantaneous transitions from one energy surface to another. Different hopping criteria result in many variants of this method. For example, in [37], an algorithm with "fewest" hoppings was developed. The hoppings in that paper were performed in a Monte Carlo procedure based on the transition rates. For a review of surface hopping methods see [6].

In recent years, Horenko *et al.* adopted the partial Wigner transform to reduce a full quantum dynamics into the quantum-classical Liouville equation, and then used

the surface hopping approach to evolve the Gaussian phase space packets. For the single avoided crossing cases, they demonstrated that the convergence towards full quantum mechanical dynamics of their method was faster than Tully's methods [14]. Kammerer, Lasser, and Teufel analyzed the propagation through conical surface crossings using the Wigner transform and Wigner measures [30, 22] and proposed a rigorous surface hopping method based on the semiclassical limit of the time-dependent Born–Oppenheimer approximation. They used the particle method to solve the Liouville equation [29, 25]. Each classical trajectory was subject to a deterministic branching process. Branching occurrs whenever a trajectory attains one of its local minimal gaps between the eigenvalue surfaces. The new branches are reweighted according to the Landau–Zener formula for conical crossings.

These classical Lagrangian surface hopping methods are very simple to implement, and in particular, very efficient in high space dimension. However, they require either many statistical samples in a Monte Carlo framework, or the increase of particle numbers whenever hopping occurs. In addition, in typical Lagrangian type methods, when the particle trajectories diverge, a complicated numerical reinterpolation procedure is needed to maintain a uniform accuracy in time.

In this paper, we propose an Eulerian surface hopping method for two-level Schrödinger equations with conical crossing. This method is based on the semiclassical limit of the Born–Oppenheimer approximation, namely, the system of linear Liouville equations. These Liouville equations for different energy levels are decoupled unless near the hopping zone, where the transition process, determined by the Landau–Zener formula, is modeled by an interface condition. This interface condition can be incorporated into the numerical flux of the Liouville solver, in the same way as was done for partial transmission and reflection of high frequency waves across an interface or barrier [20, 19, 16, 15]. The advantage of this Eulerian method is that, regardless of the number of times hopping occurs, the number of Liouville equations to be solved remains the same. This PDE based Eulerian numerical method also allows a uniform discretization accuracy.

This paper is organized as follows. In section 2, we recall the Wigner transform approach to obtain the semiclassical limit of the two-level Schrödinger equation and present the Landau–Zener formula for the transition rate at conical crossing between different energy level surfaces. In section 3, we present our Eulerian setup for surface hopping, the interface condition that models the Landau–Zener transition, and the numerical discretization. The positivity and l_1-stability of the scheme are proved. Numerical examples are given in section 4 to verify the convergence and accuracy of the proposed method. We make some concluding remarks in section 5.

2. The surface hopping method.

2.1. A two-level Schrödinger equation. Consider a typical case, i.e., the time-dependent two-level diabatic system of Schrödinger equations (11) with $N = 2$ [34]:

$$i\varepsilon\partial_t\psi^\epsilon(t,\mathbf{x}) = \left(-\frac{\varepsilon^2}{2}\Delta_{\mathbf{x}} + V(\mathbf{x})\right)\psi^\varepsilon(t,\mathbf{x}), \quad (t,\mathbf{x}) \in \mathbb{R}^+ \times \mathbb{R}^2, \tag{12}$$

$$\psi^\varepsilon(0,\mathbf{x}) = \psi_0^\varepsilon(\mathbf{x}) \in \mathbf{L}^2(\mathbb{R}^2,\mathbb{C}^2). \tag{13}$$

Here $\psi^\varepsilon(t,\mathbf{x}) \in \mathbb{C}^2$ is the vector wave equation, $\mathbf{x} = (x, \quad y)$, $\Delta_{\mathbf{x}} = \mathtt{diag}(\partial_x^2 + \partial_y^2, \quad \partial_x^2 + \partial_y^2)$, and $V(\mathbf{x})$ is the real symmetric potential matrix,

$$V(\mathbf{x}) = \frac{1}{2}\mathrm{tr}V(\mathbf{x}) + \begin{pmatrix} v_1(\mathbf{x}) & v_2(\mathbf{x}) \\ v_2(\mathbf{x}) & -v_1(\mathbf{x}) \end{pmatrix}. \tag{14}$$

The Hamiltonian is given by $H = -\frac{\varepsilon^2}{2}\Delta_{\mathbf{x}} + V(\mathbf{x})$. The dimensionless semiclassical parameter $\varepsilon > 0$ is given by $\varepsilon = \sqrt{\frac{m}{M}}$, where m and M are the masses of an electron and a nucleus, respectively. Then, all oscillations are roughly characterized by the frequency $1/\varepsilon$, which typically ranges between 100 and 1,000. Hereafter, we will treat ε as a small parameter and discuss the semiclassical limit of the Schrödinger equations (12) and (13).

The potential $V(\mathbf{x})$ has eigenvalues $\lambda^{(\pm)} = \mathrm{tr}V(\mathbf{x}) \pm \sqrt{v_1(\mathbf{x})^2 + v_2(\mathbf{x})^2}$. Two energy levels are called *crossing at a point* $\mathbf{x}_* \in \mathbb{R}^2$ if $\lambda^+(\mathbf{x}_*) = \lambda^-(\mathbf{x}_*)$. Such a crossing is called *conical* if the vectors $\nabla_{\mathbf{x}} v_1(\mathbf{x}_*)$ and $\nabla_{\mathbf{x}} v_2(\mathbf{x}_*)$ are linearly independent. If all the crossings are conical, the crossing set $S = \{\mathbf{x} \in \mathbb{R}^2 | \lambda^+(\mathbf{x}) = \lambda^-(\mathbf{x})\}$ is a submanifold of *codimension two* in $\mathbb{R}^2$ [11].

2.2. The semiclassical limit. In this section, we discuss the semiclassical limit of the Schrödinger equations (12), (13). Denote $\mathbf{x} = (x, y) \in \mathbb{R}^2$ and $\mathbf{k} = (\xi, \eta) \in \mathbb{R}^2$. Introduce the Wigner function [39]:

$$W^\varepsilon(\psi^\varepsilon)(\mathbf{x}, \mathbf{k}) = (2\pi)^{-2} \int_{\mathbb{R}^2} e^{i\mathbf{y}\cdot\mathbf{k}} \psi^\varepsilon \left(\mathbf{x} - \frac{\varepsilon}{2}\mathbf{y}\right) \otimes \bar{\psi}^\epsilon(\mathbf{x} + \frac{\varepsilon}{2}\mathbf{y}) d\mathbf{y}, \quad (\mathbf{x}, \mathbf{k}) \in \mathbb{R}^2_{\mathbf{x}} \times \mathbb{R}^2_{\mathbf{k}}.$$

Note that, although the Winger function W^ε cannot recover the wave function ψ^ε, the moments of W^ε give the physical observables including the position density, flux, and energy. The Wigner function is a convenient tool to study the semiclassical limit of the Schrödinger equation [39, 8, 32]. Let u denote this weak limit (in the distributional sense),

$$\lim_{\varepsilon \to 0} W^\varepsilon(t, \mathbf{x}, \mathbf{k}) \rightharpoonup u(t, \mathbf{x}, \mathbf{k}),$$

which is called the *Wigner measure* or *semiclassical measure*. We now precisely describe this limit.

First, for the Schrödinger equation (12), the complex 2×2 matrix-valued symbol is given by

$$P(\mathbf{x}, \mathbf{k}) = \frac{i}{2}|\mathbf{k}|^2 + iV(\mathbf{x}),$$

where $\mathbf{k}$ is the conjugate variable to the position variable $\mathbf{x}$. The two eigenvalues of $-iP(\mathbf{x}, \mathbf{k})$ are

$$\lambda_1(\mathbf{x}, \mathbf{k}) = \frac{|\mathbf{k}|^2}{2} + \mathrm{tr}V(\mathbf{x}) + \sqrt{v_1(\mathbf{x})^2 + v_2(\mathbf{x})^2},$$

and

$$\lambda_2(\mathbf{x}, \mathbf{k}) = \frac{|\mathbf{k}|^2}{2} + \mathrm{tr}V(\mathbf{x}) - \sqrt{v_1(\mathbf{x})^2 + v_2(\mathbf{x})^2}.$$

These eigenvalues λ_τ, $\tau = 1, 2$, in the semiclassical limit as described below by (15) (see also (18, (19)) become the Hamiltonians of the classical particles corresponding to the two energy levels, respectively. We assume that the Hamiltonian flows with Hamiltonians λ_τ leave invariant the set

$$\Omega = (\mathbb{R}^2_{\mathbf{x}} \times \mathbb{R}^2_{\mathbf{k}}) \backslash S.$$

For $(\mathbf{x},\mathbf{k}) \in \Omega$, we denote by $\chi_\tau(\mathbf{x},\mathbf{k})$ the column eigenvector corresponding to the eigenvalue $\lambda_\tau(\mathbf{x},\mathbf{k})$ and the matrix $\Pi_\tau(\mathbf{x},\mathbf{k}) = \chi_\tau(\mathbf{x},\mathbf{k})(\chi_\tau(\mathbf{x},\mathbf{k}))^T$ is the orthogonal projection onto the eigenspace associated to $\lambda_\tau(\mathbf{x},\mathbf{k})$.

By Theorem 6.1 of [8], outside the crossing set S, the Wigner measure $u(t,\cdot)$ commutes with the projectors Π_τ and thus can be decomposed as

$$u(t,\cdot) = \Pi_1 u(t,\cdot)\Pi_1 + \Pi_2 u(t,\cdot)\Pi_2.$$

Since the eigenspaces are one-dimensional, the decomposition is simplified to be

$$u(t,\cdot) = u_1(t,\cdot)\Pi_1 + u_2(t,\cdot)\Pi_2,$$

where the scalar function $u_\tau(t,\mathbf{x},\mathbf{k})$, determined by projection

$$u_\tau(t,\mathbf{x},\mathbf{k}) = \mathrm{tr}(\Pi_\tau u(t,\mathbf{x},\mathbf{k}))$$

satisfies the classical Liouville equation

$$\partial_t u_\tau + \nabla_{\mathbf{k}}\lambda_\tau \cdot \nabla_{\mathbf{x}} u_\tau - \nabla_{\mathbf{x}}\lambda_\tau \cdot \nabla_{\mathbf{k}} u_\tau = 0, \quad (t,\mathbf{x},\mathbf{k}) \in \mathbb{R}^+ \times \Omega, \tag{15}$$

$$u_\tau(0) = \mathrm{tr}(\Pi_\tau \mu_0), \quad (\mathbf{x},\mathbf{k}) \in \Omega. \tag{16}$$

The scalar functions $u_\tau(t,\mathbf{x}\ \mathbf{k}), \tau = 1,2$ are the phase space probability densities corresponding to the upper and lower energy level, respectively. One can recover the electron densities $U_1(t,\mathbf{x})$ and $U_2(t,\mathbf{x})$ in the physical space by taking the moments,

$$U_\tau(t,\mathbf{x}) = \int_{R^2_{\mathbf{k}}} u_\tau(t,\mathbf{x},\mathbf{k}) d\mathbf{k}, \quad \tau = 1,2. \tag{17}$$

Therefore, the Liouville equations (15) in phase space give the propagation of the Wigner measures $u_1(t,\cdot)$ and $u_2(t,\cdot)$ on any given time interval, provided that their supports do not intersect the eigenvalue crossing set S.

The computational challenge arises when their support set intersects the eigenvalue crossing set S, where the Liouville equations corresponding to $u_1(t,\cdot)$ and $u_2(t,\cdot)$ are not valid. Thus a crossing condition at S should be provided to account for the nonadiabatic transition between the two energy levels.

2.3. The Landau–Zener formula. In [29], there was a heuristic derivation of the nonadiabatic transition probability between $u_1(t,\cdot)$ and $u_2(t,\cdot)$ at S. The derivation is based on the Hamiltonian system corresponding to the Liouville equations (15)

$$\dot{\mathbf{x}}_\tau(t) = \nabla_{\mathbf{k}}\lambda_\tau(t) = \mathbf{k}_\tau(t), \tag{18}$$

$$\dot{\mathbf{k}}_\tau(t) = -\nabla_{\mathbf{x}}\lambda_\tau(t), \quad \tau = 1,2, \tag{19}$$

where $\mathbf{x}_\tau(t) = (x_\tau(t), y_\tau(t)) \in \mathbb{R}^2_{\mathbf{x}}$ and $\mathbf{k}_\tau(t) = (\xi_\tau(t), \eta_\tau(t)) \in \mathbb{R}^2_{\mathbf{k}}$ are the position and velocity of particles with density distribution u_τ. The basic idea is to insert the trajectories $(\mathbf{x}(t),\mathbf{k}(t))$ of the Hamiltonian systems (18) and (19) into the trace-free part of the potential matrix (14) and obtain an ordinary differential system,

$$i\varepsilon\frac{d}{dt}\psi(t) = \begin{pmatrix} v_1(\mathbf{x}(t)) & v_2(\mathbf{x}(t)) \\ v_2(\mathbf{x}(t)) & -v_1(\mathbf{x}(t)) \end{pmatrix}\psi(t).$$

The nonadiabatic transitions between u_1 and u_2 happen in the region where the gap between the eigenvalues becomes minimal. The function

$$h(\mathbf{x}(t)) = |\lambda_1(\mathbf{x}(t)) - \lambda_2(\mathbf{x}(t))| = 2|\mathbf{v}(\mathbf{x}(t))|$$

measures the gap between the eigenvalues in phase space along the classical trajectory $(\mathbf{x}(t), \mathbf{k}(t))$, where $\mathbf{v}(\mathbf{x}) = (v_1(\mathbf{x}), v_2(\mathbf{x}))$ is a vector and $|\cdot|$ is the Euclidean norm. The necessary condition for a trajectory to attain the minimal gap is given by,

$$\frac{d}{dt}|\mathbf{v}(\mathbf{x}(t))|^2 = \mathbf{v}(\mathbf{x}(t)) \cdot \nabla_{\mathbf{x}}\mathbf{v}(\mathbf{x}(t))\mathbf{k}(t) = 0,$$

where $\nabla_{\mathbf{x}}\mathbf{v}(\mathbf{x}(t)$ is the Jacobian matrix of vector $\mathbf{v}(\mathbf{x}(t))$, and $\mathbf{k}(t) = \dot{\mathbf{x}}(t)$. Hence, a crossing manifold in the phase space containing these points of the minimal gaps is

$$S^* = \left\{(\mathbf{x}, \mathbf{k}) \in \mathbb{R}^2_{\mathbf{x}} \times \mathbb{R}^2_{\mathbf{k}} \middle| \mathbf{v}(\mathbf{x}(t)) \cdot \nabla_{\mathbf{x}}\mathbf{v}(\mathbf{x}(t))\mathbf{k}(t) = 0\right\}.$$

The transition probability when one particle hits S^* is obtained as (refer to [29])

$$T(\mathbf{x}_0, \mathbf{k}_0) = \exp\left(-\frac{\pi}{\varepsilon}\frac{(\mathbf{v}(\mathbf{x}_0) \wedge \nabla_{\mathbf{x}}\mathbf{v}(\mathbf{x}_0)\mathbf{k}_0)^2}{|\nabla_{\mathbf{x}}\mathbf{v}(\mathbf{x}_0)\mathbf{k}_0|^3}\right), \tag{20}$$

which is the famous *Landau–Zener formula* [26, 41]. Here the wedge product is defined as $\mathbf{v} \wedge \mathbf{w} = v_2 w_1 - v_1 w_2$ for $\mathbf{v}$ and $\mathbf{w} \in \mathbb{R}^2$.

Notice that T decays exponentially in $\mathbf{x}$ and $\mathbf{k}$. When $\varepsilon \to 0$,

$$T \to T_0 = \begin{cases} 1, & (\mathbf{x}, \mathbf{k}) \in S = \{(0,0)\}, \\ 0, & (\mathbf{x}, \mathbf{k}) \notin S, \end{cases}$$

which means when $\varepsilon \to 0$, the hopping only occurs on S. It is consistent with the result in the previous subsections.

3. An Eulerian method.

3.1. An Eulerian setup. Our Eulerian framework consists of solving the two Liouville equations

$$\partial_t u_\tau + \nabla_{\mathbf{k}}\lambda_\tau \cdot \nabla_{\mathbf{x}} u_\tau - \nabla_{\mathbf{x}}\lambda_\tau \cdot \nabla_{\mathbf{k}} u_\tau = 0, \quad (t, \mathbf{x}, \mathbf{k}) \in R^+ \times \Omega, \quad \tau = 1, 2$$

with an interface condition that incorporates the Landau–Zener transition. Note that the Schrödinger equation (12) has the conservation of total mass

$$\partial_t \int |\psi^\epsilon|^2 \, d\mathbf{x} = 0, \tag{21}$$

which gives, in the semiclassical limit $\epsilon \to 0$,

$$\partial_t \int (u_1 + u_2) \, d\mathbf{k} \, d\mathbf{x} = 0. \tag{22}$$

For this condition to hold, *the flux needs to be continuous across the hopping surface* S^*. Thus the Landau–Zener transition at S^* should be formulated as a continuity condition for the flux in the normal direction to S^*. Define the flux

$$j_\tau(\mathbf{x}, \mathbf{k}) = (\nabla_{\mathbf{k}}\lambda_\tau, -\nabla_{\mathbf{x}}\lambda_\tau)\, u_\tau(\mathbf{x}, \mathbf{k}), \quad \tau = 1, 2\,.$$

Then the interface condition is

$$\begin{pmatrix} j_1(\mathbf{x}_0^+,\mathbf{k}_0^+)\cdot\vec{n} \\ j_2(\mathbf{x}_0^+,\mathbf{k}_0^+)\cdot\vec{n} \end{pmatrix} = \begin{pmatrix} 1-T(\mathbf{x}_0,\mathbf{k}_0) & T(\mathbf{x}_0,\mathbf{k}_0) \\ T(\mathbf{x}_0,\mathbf{k}_0) & 1-T(\mathbf{x}_0,\mathbf{k}_0) \end{pmatrix} \begin{pmatrix} j_1(\mathbf{x}_0^-,\mathbf{k}_0^-)\cdot\vec{n} \\ j_2(\mathbf{x}_0^-,\mathbf{k}_0^-)\cdot\vec{n} \end{pmatrix}, \tag{23}$$

where $(\mathbf{x}^\pm,\mathbf{k}^\pm)$ are the limits to $(\mathbf{x}_0,\mathbf{k}_0)\in S^*$ along $\vec{n}$, the normal direction to the hopping surface S^*.

It should be pointed out that this interface condition, due to the validity of the Landau–Zener probability, only works in the following two cases:

(1) $u_1(\mathbf{x}_0^-,\mathbf{k}_0^-)\neq 0$ and $u_2(\mathbf{x}_0^-,\mathbf{k}_0^-)=0$,

(2) $u_1(\mathbf{x}_0^-,\mathbf{k}_0^-)=0$ and $u_2(\mathbf{x}_0^-,\mathbf{k}_0^-)\neq 0$.

The interference resulted when two particles from different energy level surfaces arrive at S^* at the same time is not accounted for. This is a restriction of any method based on Laudau–Zener transition probability.

3.2. The numerical fluxes. In this section we describe the finite volume scheme for the two-dimensional (2D) Liouville equation

$$\frac{\partial u_\tau}{\partial t}+\xi\frac{\partial u_\tau}{\partial x}+\eta\frac{\partial u_\tau}{\partial y}-\frac{\partial \lambda_\tau}{\partial x}\frac{\partial u_\tau}{\partial \xi}-\frac{\partial \lambda_\tau}{\partial y}\frac{\partial u_\tau}{\partial \eta}=0,\quad \tau=1,2. \tag{24}$$

Without loss of generality, we employ the finite volume method with a uniform mesh. Suppose h_x, h_y, h_ξ, $h_\eta>0$ are mesh sizes. In each direction, the mesh points are at $(x_{i+\frac12},y_{j+\frac12},\xi_{k+\frac12},\eta_{l+\frac12})$, satisfying $x_{i+\frac12}-x_{i-\frac12}=h_x$, $y_{j+\frac12}-y_{j-\frac12}=h_y$, $\xi_{k+\frac12}-\xi_{k-\frac12}=h_\xi$, and $\eta_{l+\frac12}-\eta_{l-\frac12}=h_\eta$. The cells are centered at (x_i,y_j,ξ_k,η_l), where $x_i=\frac12(x_{i-\frac12}+x_{i+\frac12})$, $y_j=\frac12(y_{j-\frac12}+y_{j+\frac12})$, $\xi_k=\frac12(\xi_{k-\frac12}+\xi_{k+\frac12})$, $\eta_l=\frac12(\eta_{l-\frac12}+\eta_{l+\frac12})$. We do not discretize in time now so that we can choose different schemes, such as Runge–Kutta methods, in time for different accuracy requirements. The cell averages of $(u_\tau)^n_{ijkl}$ are defined by

$$(u_\tau)_{ijkl}=\frac{1}{h_xh_yh_\xi h_\eta}\int_{x_{i-\frac12}}^{x_{i+\frac12}}\int_{y_{j-\frac12}}^{y_{j+\frac12}}\int_{\xi_{k-\frac12}}^{\xi_{k+\frac12}}\int_{\eta_{l-\frac12}}^{\eta_{l+\frac12}}u_\tau(x,y,\xi,\eta,t)d\eta d\xi dy dx,\quad \tau=1,2.$$

The Liouville equations (24) then can be discretized as

$$\begin{aligned}\Big[(u_\tau)_{ijkl}\Big]_t=&-\frac{1}{h_x}\xi_k\left((u_\tau)^-_{i+\frac12,jkl}-(u_\tau)^+_{i-\frac12,jkl}\right)\\&-\frac{1}{h_y}\eta_l\left((u_\tau)^-_{i,j+\frac12,kl}-(u_\tau)^+_{i,j-\frac12,kl}\right)\\&+\frac{1}{h_\xi}\frac{\partial\lambda_\tau}{\partial x}(x_i,y_j)\left((u_\tau)^-_{ij,k+\frac12,l}-(u_\tau)^+_{ij,k-\frac12,l}\right)\\&+\frac{1}{h_\eta}\frac{\partial\lambda_\tau}{\partial y}(x_i,y_j)\left((u_\tau)^-_{ijk,l+\frac12}-(u_\tau)^+_{ijk,l-\frac12}\right).\end{aligned} \tag{25}$$

For points away from S^*, the numerical flux in (25) is given by the upwind scheme (which is quite diffusive) or its high resolution extension using slope limiters [31] (which offers much better numerical resolution than its first order counterpart). Since no hopping occurs, the fluxes are continuous. For example, at $x=x_{i+\frac12}$, $(u_\tau)^-_{i+\frac12,jkl}=(u_\tau)^+_{i+\frac12,jkl}$, $\tau=1,2$. In other directions, the fluxes are defined similarly.

Now we introduce the interface condition for the numerical flux on S^*. Recall that S^* is given by

$$S^* = \left\{(\mathbf{x},\mathbf{k}) \in R^2_{\mathbf{x}} \times R^2_{\mathbf{k}} \middle| v(\mathbf{x}) \cdot \nabla_{\mathbf{x}} v(\mathbf{x})\mathbf{k} = 0\right\}, \quad \mathbf{x} = (x,y), \quad \mathbf{k} = (\xi,\eta),$$

which is a curved surface in the phase space $R^2_{\mathbf{x}} \times R^2_{\mathbf{k}}$. In order to design a numerical scheme, we will approximate this curved surface by the closest points on the mesh, similar to what was done in [15]. In [15] the authors used a dimension-by-dimension sweeping to detect the interface. Here we adopt the same approach to approximate S^* in four-dimensional (4D) phase space. First define a function

$$F(x,y,\xi,\eta) = v(\mathbf{x}) \cdot \nabla_{\mathbf{x}} v(\mathbf{x})\mathbf{k}, \quad \mathbf{x} = (x,y), \quad \mathbf{k} = (\xi,\eta).$$

In the x-direction, we check the sign of $D_{i+\frac{1}{2}} = F(x_i, y_j, \xi_k, \eta_l)F(x_{i+1}, y_j, \xi_k, \eta_l)$ for all i. If $D_{i+\frac{1}{2}} \le 0$, we assume there is an interface point at $x = x_{i+\frac{1}{2}}$. This of course introduces an $O(h_x)$ error, but for a Cartesian grid we will tolerate such an error. For other directions, similar sweeping process can determine the approximate location of S^* in the corresponding direction.

We here just assume u_1 is nonzero and u_2 vanishes. The case when u_1 vanishes and u_2 is nonzero can be obtained similarly. At S^*, part of the density associated with u_1 will be redistributed to u_2 due to hopping. We approximate the hopping probabilities by the Landau–Zener formula (20), which take values at the cell centers, as $T_{ijkl} = T(x_i, y_j, \xi_k, \eta_l)$ with T given by (20).

In the following, we will explain how to define the numerical fluxes $(u_\tau)^{\pm}_{i+\frac{1}{2},jkl}$, $(u_\tau)^{\pm}_{ij,k+\frac{1}{2},l}$, $\tau = 1,2$ on the interface. The numerical fluxes $(u_\tau)^{\pm}_{i,j+\frac{1}{2},kl}$, $(u_\tau)^{n,\pm}_{ijk,l+\frac{1}{2}}$, $\tau = 1,2$ are defined similarly.

Numerical fluxes at S^*.

If $(x_{i+\frac{1}{2}}, y_j, \xi_k, \eta_l)$ is on the interface, then in the x direction,

for $(u_1)^{\pm}_{i+\frac{1}{2},jkl}$,

1. if $\xi_k \ge 0$,

$(u_1)^{-}_{i+\frac{1}{2},jkl} = (u_1)_{ijkl} + \frac{1}{2}h_x(\sigma_1)_{\underline{i},jkl}, \quad (u_1)^{+}_{i+\frac{1}{2},jkl} = (1 - T_{ijkl})\,(u_1)^{-}_{i+\frac{1}{2},jkl}$;

2. if $\xi_k < 0$,

$(u_1)^{+}_{i+\frac{1}{2},jkl} = (u_1)_{i+1,jkl} - \frac{1}{2}h_x(\sigma_1)_{\underline{i+1},jkl}$, $(u_1)^{-}_{i+\frac{1}{2},jkl} = (1 - T_{ijkl})\,(u_1)^{+}_{i+\frac{1}{2},jkl}$;

for $(u_2)^{\pm}_{i+\frac{1}{2},jkl}$,

1. if $\xi_k \ge 0$,

$(u_2)^{-}_{i+\frac{1}{2},jkl} = (u_2)_{ijkl} + \frac{1}{2}h_x(\sigma_2)_{\underline{i},jkl}$,

$(u_2)^{+}_{i+\frac{1}{2},jkl} = (u_2)^{-}_{i+\frac{1}{2},jkl} + T_{ijkl}\,(u_1)^{-}_{i+\frac{1}{2},jkl}$;

2. if $\xi_k < 0$,

$(u_2)^{+}_{i+\frac{1}{2},jkl} = (u_2)_{i+1,jkl} - \frac{1}{2}h_x(\sigma_2)_{\underline{i+1},jkl}$,

$(u_2)^{-}_{i+\frac{1}{2},jkl} = (u_2)^{+}_{i+\frac{1}{2},jkl} + T_{ijkl}\,(u_1)^{+}_{i+\frac{1}{2},jkl}$.

If $(x_i, y_j, \xi_{k+\frac{1}{2}}, \eta_l)$ is on the interface, then in the ξ direction,

for $(u_1)^{\pm}_{ij,k+\frac{1}{2},l}$,

1. if $-\frac{\partial \lambda_1}{\partial x}(x_i, y_j) \ge 0$,

$(u_1)^{-}_{ij,k+\frac{1}{2},l} = (u_1)_{ijkl} + \frac{1}{2}h_\xi(\sigma_1)_{ij,\underline{k},l}$,

$(u_1)^{+}_{ij,k+\frac{1}{2},l} = (1 - T_{ijkl})\,(u_1)^{-}_{ij,k+\frac{1}{2},l}$;

2. if $-\frac{\partial \lambda_1}{\partial x}(x_i, y_j) < 0$,
$(u_1)^+_{ij,k+\frac{1}{2},l} = (u_1)_{ij,k+1,l} - \frac{1}{2} h_\xi (\sigma_1)_{ij,\underline{k+1},l}$,
$(u_1)^-_{ij,k+\frac{1}{2},l} = (1 - T_{ijkl})\,(u_1)^+_{ij,k+\frac{1}{2},l}$;
for $(u_2)^\pm_{ij,k+\frac{1}{2},l}$,
1. if $-\frac{\partial \lambda_2}{\partial x}(x_i, y_j) \geq 0$,
$(u_2)^-_{ij,k+\frac{1}{2},l} = (u_2)_{ijkl} + \frac{1}{2} h_\xi (\sigma_2)_{ij,\underline{k},l}$,
$(u_2)^+_{ij,k+\frac{1}{2},l} = (u_2)^-_{ij,k+\frac{1}{2},l} + A_{ijkl} \left| \frac{\partial \lambda_1}{\partial x} / \frac{\partial \lambda_2}{\partial x} \right|$;
2. if $-\frac{\partial \lambda_2}{\partial x}(x_i, y_j) < 0$,
$(u_2)^+_{ij,k+\frac{1}{2},l} = (u_2)_{ij,k+1,l} - \frac{1}{2} h_\xi (\sigma_2)_{ij,\underline{k+1},l}$,
$(u_2)^-_{ij,k+\frac{1}{2},l} = (u_2)^+_{ij,k+\frac{1}{2},l} + A_{ijkl} \left| \frac{\partial \lambda_1}{\partial x} / \frac{\partial \lambda_2}{\partial x} \right|$,
where

$$A_{ijkl} = \begin{cases} T_{ijkl}\,(u_1)^-_{ij,k+\frac{1}{2},l}, & \text{when } -\frac{\partial \lambda_1}{\partial x}(x_i, y_j) \geq 0, \\ T_{ijkl}\,(u_1)^+_{ij,k+\frac{1}{2},l}, & \text{when } -\frac{\partial \lambda_1}{\partial x}(x_i, y_j) < 0. \end{cases}$$

Note that in the numerical flux in the direction of ξ, the term $\left| \frac{\partial \lambda_1}{\partial x} / \frac{\partial \lambda_2}{\partial x} \right|$ is to reflect the interface condition (23) in the ξ-direction; namely, the flux in the normal direction to the interface is continuous.

Here $(\sigma_\tau)_{\underline{i}jkl}$ is the slope of u_1 in the cell centered at $(x_i, y_j, \xi_k, \eta_l)$ in x-direction and $(\sigma_\tau)_{ij\underline{k}l}$ in ξ direction. One possible choice is the *monotonized central-difference limiter*, which can be defined by

$$(\sigma_\tau)^n_{\underline{i}jkl} = \text{minmod}\left(\frac{(u_\tau)^n_{i+1,jkl} - (u_\tau)^n_{i-1,jkl}}{2h_x}, 2\frac{(u_\tau)^n_{i+1,jkl} - (u_\tau)^n_{i,jkl}}{h_x}, 2\frac{(u_\tau)^n_{i,jkl} - (u_\tau)^n_{i-1,jkl}}{h_x} \right). \tag{26}$$

The definitions of other slopes are similar. In general, one probably needs to modify slope limiter near the interface by using the Hamiltonian-preserving principle across the interface, as in [21]. For the numerical examples in the next section, we just use the monotonized central-difference limiter, which works well for our examples; therefore we do not consider this issue here.

The time discretization can be any numerical ODE solver.

Remark 3.1. In the Hamiltonian-preserving schemes (see [15, 19, 18]), when the transmissions happen on the interface, one needs to adjust the momenta in order to conserve the total Hamiltonian. In this paper, since the probability in the Landau–Zener formula (20) decays exponentially, most of the hoppings happen in the neighborhood of the crossing point, where the energy difference between two potential energy surfaces is negligible. Therefore we do not consider the adjustment of momentum here. However, the momentum adjustment is sometimes necessary and it will be addressed in our future work.

3.3. Positivity and l_1 stability. It is important for the numerical scheme to guarantee the positivity of density distributions u_1 and u_2 when solving the Liouville equations (24) with (23). We now prove this property for the first order scheme.

Consider the scheme for (24) with (23) using the first order numerical flux, and the forward Euler method in time. Let

$$\alpha_{ijkl} = \begin{cases} 0, & (x_i, y_j, \xi_k, \eta_l) \in \mathbb{R}^2_{\mathbf{x}} \times \mathbb{R}^2_{\mathbf{k}} \backslash S^*, \\ T_{ijkl}, & (x_i, y_j, \xi_k, \eta_l) \in S^* \end{cases}$$

be the indicator, which equals the Landau–Zener formula T_{ijkl} on the crossing set S^*, and vanishes away from S^*. For simplicity, we only consider the case $\xi_k > 0$, $\eta_l > 0$, $\frac{\partial \lambda_1}{\partial x}(x_i, y_j) < 0$, $\frac{\partial \lambda_1}{\partial y}(x_i, y_j) < 0$, $\frac{\partial \lambda_2}{\partial x}(x_i, y_j) > 0$, and $\frac{\partial \lambda_2}{\partial y}(x_i, y_j) > 0$. The other cases can be treated similarly with the same conclusion. The scheme (25) for u_1 and u_2 becomes

$$\begin{aligned} (u_1)^{n+1}_{ijkl} =& (u_1)^n_{ijkl} - \frac{\Delta t}{h_x}\xi_k \left((u_1)^n_{ijkl} - (1 - \alpha_{i-1,jkl}) (u_1)^n_{i-1,jkl} \right) \\ & - \frac{\Delta t}{h_y}\eta_l \left((u_1)^n_{ijkl} - (1 - \alpha_{i,j-1,kl}) (u_1)^n_{i,j-1,kl} \right) \\ & + \frac{\Delta t}{h_\xi}\frac{\partial \lambda_1}{\partial x}(x_i, y_j) \left((u_1)^n_{ijkl} - (1 - \alpha_{ij,k-1,l}) (u_1)^n_{ij,k-1,l} \right) \\ & + \frac{\Delta t}{h_\eta}\frac{\partial \lambda_1}{\partial y}(x_i, y_j) \left((u_1)^n_{ijkl} - (1 - \alpha_{ijk,l-1}) (u_1)^n_{ijk,l-1} \right), \end{aligned} \tag{27}$$

(28)

$$\begin{aligned} (u_2)^{n+1}_{ijkl} =& (u_2)^n_{ijkl} - \frac{\Delta t}{h_x}\xi_k \left((u_2)^n_{ijkl} - \left(\alpha_{i-1,jkl} (u_1)^n_{i-1,jkl} + (u_2)^n_{i-1,jkl} \right) \right) \\ & - \frac{\Delta t}{h_y}\eta_l \left((u_2)^n_{ijkl} - \left(\alpha_{i,j-1,kl} (u_1)^n_{i,j-1,kl} + (u_2)^n_{i,j-1,kl} \right) \right) \\ & + \frac{\Delta t}{h_\xi}\frac{\partial \lambda_2}{\partial x}(x_i, y_j) \left(\left| \frac{\partial \lambda_1}{\partial x} / \frac{\partial \lambda_2}{\partial x} \right| \alpha_{ij,k+1,l} (u_1)^n_{ij,k+1,l} + (u_2)^n_{ij,k+1,l} - (u_2)^n_{ijkl} \right) \\ & + \frac{\Delta t}{h_\eta}\frac{\partial \lambda_2}{\partial y}(x_i, y_j) \left(\left| \frac{\partial \lambda_1}{\partial y} / \frac{\partial \lambda_2}{\partial y} \right| \alpha_{ijk,l+1} (u_1)^n_{ijk,l+1} + (u_2)^n_{ijk,l+1} - (u_2)^n_{ijkl} \right), \end{aligned}$$

They can be rewritten as

$$\begin{aligned} (u_1)^{n+1}_{ijkl} =& \left(1 - \frac{\Delta t}{h_x}\xi_k - \frac{\Delta t}{h_y}\eta_l + \frac{\Delta t}{h_\xi}\frac{\partial \lambda_1}{\partial x}(x_i, y_j) + \frac{\Delta t}{h_\eta}\frac{\partial \lambda_1}{\partial y}(x_i, y_j) \right) (u_1)^n_{ijkl} \\ & + \frac{\Delta t}{h_x}\xi_k (1 - \alpha_{i-1,jkl}) (u_1)^n_{i-1,jkl} + \frac{\Delta t}{h_y}\eta_l (1 - \alpha_{i,j-1,kl}) (u_1)^n_{i,j-1,kl} \\ & - \frac{\Delta t}{h_\xi}\frac{\partial \lambda_1}{\partial x}(x_i, y_j)(1 - \alpha_{ij,k-1,l}) (u_1)^n_{ij,k-1,l} \\ & - \frac{\Delta t}{h_\eta}\frac{\partial \lambda_1}{\partial y}(x_i, y_j)(1 - \alpha_{ijk,l-1}) (u_1)^n_{ijk,l-1}, \end{aligned} \tag{29}$$

$$\begin{aligned} (u_2)^{n+1}_{ijkl} =& \left(1 - \frac{\Delta t}{h_x}\xi_k - \frac{\Delta t}{h_y}\eta_l - \frac{\Delta t}{h_\xi}\frac{\partial \lambda_2}{\partial x}(x_i, y_j) - \frac{\Delta t}{h_\eta}\frac{\partial \lambda_2}{\partial y}(x_i, y_j) \right) (u_2)^n_{ijkl} \\ & + \frac{\Delta t}{h_x}\xi_k \left(\alpha_{i-1,jkl} (u_1)^n_{i-1,jkl} + (u_2)^n_{i-1,jkl} \right) \\ & + \frac{\Delta t}{h_y}\eta_l \left(\alpha_{i,j-1,kl} (u_1)^n_{i,j-1,kl} + (u_2)^n_{i,j-1,kl} \right) \end{aligned} \tag{30}$$

$$+\frac{\Delta t}{h_\xi}\frac{\partial\lambda_2}{\partial x}(x_i,y_j)\,(u_2)^n_{ij,k+1,l}+\frac{\Delta t}{h_\xi}\left|\frac{\partial\lambda_1}{\partial x}\right|\alpha_{ij,k+1,l}\,(u_1)^n_{ij,k+1,l}$$
$$+\frac{\Delta t}{h_\eta}\frac{\partial\lambda_2}{\partial y}(x_i,y_j)\,(u_2)^n_{ijk,l+1}+\frac{\Delta t}{h_\eta}\left|\frac{\partial\lambda_1}{\partial y}\right|\alpha_{ijk,l+1}\,(u_1)^n_{ijk,l+1}$$

Now we investigate the positivity of schemes (29) and (30). This is to prove that if $(u_\tau)^n_{ijkl}\geq 0,\tau=1,2\ \forall i,j,k,l$, then it is also true for $(u_\tau)^{n+1}_{ijkl},\tau=1,2$. Clearly, one just needs to show that all coefficients for $(u_\tau)^n_{ijkl},\tau=1,2$ are nonnegative. For the case under consideration, notice that $\xi_k>0$, $\eta_l>0$, $\frac{\partial\lambda_1}{\partial x}(x_i,y_j)<0$, $\frac{\partial\lambda_1}{\partial y}(x_i,y_j)<0$, $\frac{\partial\lambda_2}{\partial x}(x_i,y_j)>0$, $\frac{\partial\lambda_2}{\partial y}(x_i,y_j)>0$, and $0\leq\alpha_{ijkl}\leq 1\ \forall i,j,k,l$.

If

$$1-\frac{\Delta t}{h_x}\xi_k-\frac{\Delta t}{h_y}\eta_l+\frac{\Delta t}{h_\xi}\frac{\partial\lambda_1}{\partial x}(x_i,y_j)+\frac{\Delta t}{h_\eta}\frac{\partial\lambda_1}{\partial y}(x_i,y_j)>0,$$
$$1-\frac{\Delta t}{h_x}\xi_k-\frac{\Delta t}{h_y}\eta_l-\frac{\Delta t}{h_\xi}\frac{\partial\lambda_2}{\partial x}(x_i,y_j)-\frac{\Delta t}{h_\eta}\frac{\partial\lambda_2}{\partial y}(x_i,y_j)>0,$$

or

$$\left(\frac{1}{h_x}\xi_k+\frac{1}{h_y}\eta_l-\frac{1}{h_\xi}\frac{\partial\lambda_1}{\partial x}(x_i,y_j)-\frac{1}{h_\eta}\frac{\partial\lambda_1}{\partial y}(x_i,y_j)\right)\Delta t<1,$$
$$\left(\frac{1}{h_x}\xi_k+\frac{1}{h_y}\eta_l+\frac{1}{h_\xi}\frac{\partial\lambda_2}{\partial x}(x_i,y_j)+\frac{1}{h_\eta}\frac{\partial\lambda_2}{\partial y}(x_i,y_j)\right)\Delta t<1,$$

then all coefficients for $(u_\tau)^n_{ijkl}\geq 0,\tau=1,2$ are nonnegative. Generally one must assume

(31)
$$\Delta t\max_{i,j,k,l}\left(\frac{1}{h_x}|\xi_k|+\frac{1}{h_y}|\eta_l|+\frac{1}{h_\xi}\left|\frac{\partial\lambda_\tau}{\partial x}(x_i,y_j)\right|+\frac{1}{h_\eta}\left|\frac{\partial\lambda_\tau}{\partial y}(x_i,y_j)\right|\right)<1,\quad \tau=1,2.$$

The scheme (25) is positive when the hyperbolic type CFL condition (31) is satisfied. Since the scheme (25) is flux conservative and positive, the l_1 stability follows easily. We can summarize the result in this section in the following theorem.

THEOREM 3.2. *For the Liouville equations* (24) *with the interface condition* (23), *when* $(u_\tau)^n_{ijkl}\geq 0,\quad \tau=1,2$, *and the CFL condition* (31) *is satisfied, the first order method described in the last subsection preserves the positivity of the solution and has the* l_1 *stability; i.e., for any* $n\geq 0$

$$(u_\tau)^n_{ijkl}\geq 0,\quad \tau=1,2,$$
$$\sum_{i,j,k,l}\left((u_1)^n_{ijkl}+(u_2)^n_{ijkl}\right)h_xh_yh_\xi h_\eta\leq\sum_{i,j,k,l}\left((u_1)^0_{ijkl}+(u_2)^0_{ijkl}\right)h_xh_yh_\xi h_\eta.$$

4. Numerical examples. In this section we present numerical examples to demonstrate the validity of the surface hopping method proposed in section 3 and to show the numerical accuracy of the numerical scheme. In the numerical computations the second order upwind shock capture method with the slope limiter (26) is used.

In our numerical experiments we choose the initial data and the potential the same as those in [29], where $u_2(0,\cdot)$, denoting initial value of the probability density for the lower energy level, vanishes. All the u_2, the probability density for the lower level, is generated from u_1, the one for the upper level, due to hopping at the crossing set S^*. The potential corresponding to the lower energy level is also designed to be repulsive so that u_2 will never come back after it leaves S^*. This way u_1 and u_2 will not arrive at the same point on the interface at the same time. Thus we do not need to concern the coherence phenomena. More general cases will be considered in our future work.

4.1. Preliminary. We consider the time-evolution of the two-level Schrödinger equations,

$$i\varepsilon\partial_t\psi^\varepsilon(t,\mathbf{x}) = \left(-\frac{\varepsilon^2}{2}\Delta_{\mathbf{x}} + V(\mathbf{x})\right)\psi^\varepsilon(t,\mathbf{x}), \quad (t,\mathbf{x}) \in \mathbb{R}^+ \times \mathbb{R}^2, \tag{32}$$

$$\psi^\varepsilon(0,\mathbf{x}) = \psi_0^\varepsilon(\mathbf{x}) \in \mathbf{L}^2(\mathbb{R}^2,\mathbb{C}^2) \tag{33}$$

with two different potentials. One is the linear isotropic potential,

$$V_{iso}(\mathbf{x}) = \begin{pmatrix} x & y \\ y & -x \end{pmatrix}, \quad \mathbf{x} = (x,y) \in \mathbb{R}^2, \tag{34}$$

and the other is the linear $E \otimes e$ Jahn–Teller potential [40],

$$V_{JT}(\mathbf{x}) = |\mathbf{x}|^2 + \begin{pmatrix} x & y \\ y & -x \end{pmatrix}, \quad \mathbf{x} = (x,y) \in \mathbb{R}^2, \tag{35}$$

which models the displacement of triatomic molecules from the equilateral triangle configuration [29].

In Figure 4.1, we depict the conical crossings of potentials V_{iso} and V_{JT} versus x and y. One can easily find that the potential energy surfaces of potentials V_{iso} and V_{JT} have the same conical crossing set $S = (0,0)$.

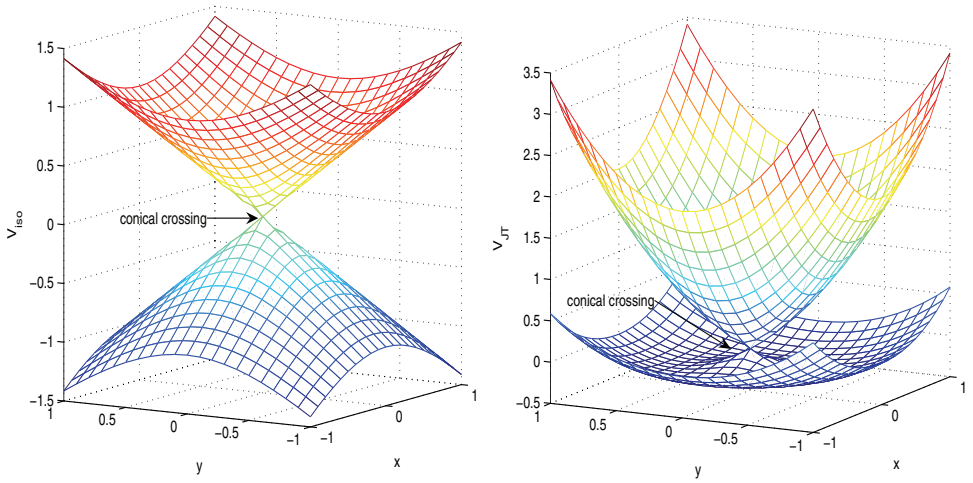

FIG. 4.1. *The conical crossings for different potentials. The left is for V_{iso}, and the right is for V_{JT}. Here the crossing point is* (0, 0).

Let $\chi_1(\mathbf{x}) = (\cos(\frac{\theta(\mathbf{x})}{2}), \quad \sin(\frac{\theta(\mathbf{x})}{2}))^T$ and $\chi_2(\mathbf{x}) = (-\sin(\frac{\theta(\mathbf{x})}{2}), \quad \cos(\frac{\theta(\mathbf{x})}{2}))^T$ denote the normalized eigenvectors of potential V_{iso} (or V_{JT}) associated with the upper and lower energy level. Here $\theta(\mathbf{x}) \in (-\pi, \pi)$ is the polar angle of $\mathbf{x} = (x, y) \in \mathbb{R}^2$.

The initial value for the two-level Schrödinger problem (32), (33) is given by

$$\psi_0^\varepsilon(\mathbf{x}) = g^\varepsilon(\mathbf{x})\chi_1(\mathbf{x}),$$

where $g_0^\varepsilon(\mathbf{x})$ is an ε-scaled Gaussian wave packet,

$$g_0^\varepsilon(\mathbf{x}) = \frac{1}{\sqrt{\pi\varepsilon}} \exp\left\{-\frac{1}{2\varepsilon}|\mathbf{x} - \mathbf{x}_0^\varepsilon|^2 + \frac{i}{\varepsilon}\mathbf{k}_0 \cdot (\mathbf{x} - \mathbf{x}_0^\epsilon)\right\},$$

which is centered at $(\mathbf{x}_0^\varepsilon, \mathbf{k}_0) \in R^2_{\mathbf{x}} \times R^2_{\mathbf{k}}$ with $||g_0^\varepsilon(\mathbf{x})||_{L^2} = 1$; see [29, 33, 13].

The Gaussian wave packet associated with the upper eigenvalue is a simple model for a molecule excited by light or a laser pulse. First, an initial wave packet is excited from the lower level (ground state) potential by a short laser pulse in the femto or nanosecond regime. This excited wave packet then evolves under the influence of the upper level (excited state) potential. Nonadiabatic transitions between adjacent potential energy surfaces will happen when this wave packet moves close to the crossing regions; see [23, 35].

The standard operator splitting spectral method is used for the Schödinger solver; see [29, 2]. We refer to the appendix for a brief description of this method.

Figure 4.2 depicts the contours of energy populations for the propagation of a Gaussian wave packet through the conical crossing with V_{iso}. The solution was obtained by the Schrödinger solver with $\varepsilon = 0.01$ and $h = \frac{1}{400}$. Initially the wave packet is only on the upper energy level. At time $t = 2\sqrt{\varepsilon}$, the Gaussian wave packet is still away from the crossing point; therefore the lower energy level is still empty. Around time $t = 4\sqrt{\varepsilon}$, the wave packet on the upper level moves near the crossing point; then part of it will hop to the lower energy level. Finally at time $t = 6\sqrt{\varepsilon}$ the hopping process finishes and the wave packets in both energy levels will move away from the crossing point.

According to the discussion in the previous section, for the surface hopping method, the crossing manifold S^* can be described by

$$S^* = \{(\mathbf{x}, \mathbf{k})|\ \mathbf{x} \cdot \mathbf{k} = 0\ \},$$

or more precisely,

$$S^* = \{(x, y, \xi, \eta)|\ x\xi + y\eta = 0\ \}.$$

This crossing manifold is a curved interface in 4D phase space and will be approximated by the adjacent interfaces using the approach discussed in section 3.2. For those potentials, V_{iso} and V_{JT}, the Landau–Zener formula (20) can be written in an explicit form,

$$T(\mathbf{x}, \mathbf{k}) = T(x, y, \xi, \eta) = \exp\left\{-\frac{\pi}{\varepsilon}\frac{(x\eta - y\xi)^2}{\sqrt[3]{\xi^2 + \eta^2}}\right\}.$$

The initial values of the corresponding Liouville equation (16) are given by

$$u_1(0, \mathbf{x}, \mathbf{k}) = \frac{1}{(\pi\varepsilon)^2} \exp\left(-\frac{1}{\varepsilon}|\mathbf{x} - \mathbf{x}_0^\varepsilon|^2 - \frac{1}{\varepsilon}|\mathbf{k} - \mathbf{k}_0|^2\right), \tag{36}$$

$$u_2(0, \mathbf{x}, \mathbf{k}) = 0, \tag{37}$$

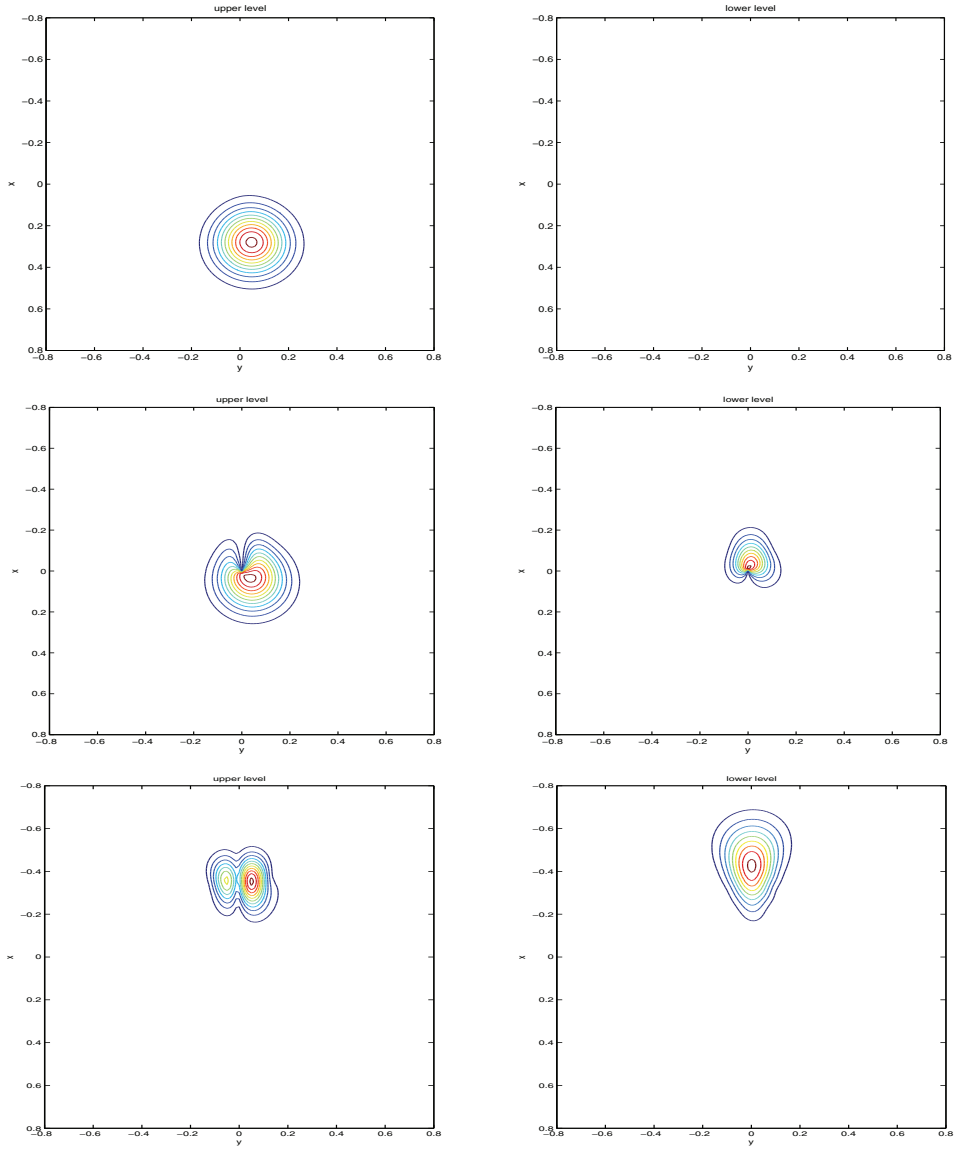

FIG. 4.2. *The plots show the energy populations for the propagation of a Gaussian wave packet through the conical crossing with V_{iso}. The solution was obtained by the Schrödinger solver with $\varepsilon = 0.01$, and $h = \frac{1}{400}$. From top to bottom, we plot $|\Pi^\tau \psi^\varepsilon(t, \mathbf{x})|^2$, $\tau = 1, 2$, $t = 2\sqrt{\varepsilon}$, $4\sqrt{\varepsilon}$, and $6\sqrt{\varepsilon}$, which correspond to pre-, during and after hopping periods. The left column corresponds to the upper level, and the right column corresponds to the lower level.*

where $u_1(0, \mathbf{x}, \mathbf{k})$ is a Gaussian given by the Wigner transform of an ε-scaled Gaussian wavepacket $\psi_0^\varepsilon(\mathbf{x})$.

In the numerical experiments, the semiclassical parameter is chosen as $\varepsilon = 10^{-k}, k = 2, 3, 4$.

The center of the initial Gaussian wave packet is chosen as (refer to [29])

$$\mathbf{x}_0^\varepsilon = \left(5\sqrt{\varepsilon}, \frac{1}{2}\sqrt{\varepsilon}\right), \quad \mathbf{k}_0 = (-1, 0) \tag{38}$$

such that the overlap of the initial Gaussian support set with the neighborhood of the crossing point $\mathbf{x} = (0, 0)$ is negligible.

The computational time is $[t_i, t_f] = [0, 10\sqrt{\varepsilon}]$. During this time, the Gaussian wave packet $\psi^\varepsilon(t, \mathbf{x})$ moves towards the crossing set. Then part of the population density will hop to the lower energy level according to the Landau–Zener formula and the other part will remain in the upper energy level. Finally the population density on both energy levels will move away from the crossing set.

Let $|\Pi^\tau \psi^\varepsilon(t, \mathbf{x})|^2$, $\tau = 1, 2$ denote the position densities of the projected wave function, where $\Pi^\tau = \chi_\tau(\mathbf{x})(\chi_\tau(\mathbf{x}))^T$, $\tau = 1, 2$ is the orthogonal projection matrix. The total population on the upper (or lower) energy level at any time t is defined by

$$P^\tau_{sch}(t) = \int_{R^2_{\mathbf{x}}} |\Pi^\tau \psi^\varepsilon(t, \mathbf{x})|^2 d\mathbf{x}, \quad \tau = 1, 2.$$

Similarly we can define the total population on the upper (or lower) energy level at any time t obtained by our Eulerian surface hopping method; that is,

$$P^\tau_{liou}(t) = \int_{R^2_{\mathbf{k}}} \int_{R^2_{\mathbf{x}}} u_\tau(t, \mathbf{x}, \mathbf{k}) d\mathbf{k} d\mathbf{x}, \quad \tau = 1, 2.$$

In the quantum dynamic simulation it is of interest to determine the final populations $P^\tau(t_f), \tau = 1, 2$ after the nonadiabatic transition, which gives the probability of finding the system in one of the two eigenspaces at time $t = t_f$. It is also of interest to find the population of the upper (or lower) level at all time, which gives the information of the whole surface hopping process. We will compare the results by solving the Schrödinger equation and the surface hopping method in the next subsection. Furthermore, the long time behavior of the surface hopping process will also be tested.

Since the total populations are conserved, i.e.,

$$P^1_{sch}(t) + P^2_{sch}(t) = 1, \quad P^1_{liou}(t) + P^2_{liou}(t) = 1 \quad \forall t > 0,$$

we only compare the upper energy level populations $P^1_{liou}(t)$ and $P^1_{sch}(t)$ in our numerical experiments. For simplicity we omit the superscript in next subsection.

4.2. Numerical results. In this section, we will consider the following two examples for the proposed numerical scheme.

Example 4.1. The propagation equations of the Wigner measures corresponding to the solution to the Schrödinger equations (32) with the linear isotropic potential V_{iso} can be written as the following Liouville equations:

$$\frac{\partial u_1}{\partial t} + \xi \frac{\partial u_1}{\partial x} + \eta \frac{\partial u_1}{\partial y} - \frac{x}{\sqrt{x^2 + y^2}} \frac{\partial u_1}{\partial \xi} - \frac{y}{\sqrt{x^2 + y^2}} \frac{\partial u_1}{\partial \eta} = 0, \tag{39}$$

$$\frac{\partial u_2}{\partial t} + \xi \frac{\partial u_2}{\partial x} + \eta \frac{\partial u_2}{\partial y} + \frac{x}{\sqrt{x^2 + y^2}} \frac{\partial u_2}{\partial \xi} + \frac{y}{\sqrt{x^2 + y^2}} \frac{\partial u_2}{\partial \eta} = 0 \tag{40}$$

with the initial values of u_1 and u_2 chosen as (36)–(38). We test the convergence of the original Schrödinger equation (32) toward the Liouville equations (39), (40) by varying the semiclassical parameter as $\varepsilon = 10^{-2}, 10^{-3}, 10^{-4}$.

The computational domain for the Liouville equations (39), (40) is chosen to be $[x, y, \xi, \eta] = [-10\sqrt{\varepsilon}, 10\sqrt{\varepsilon}] \times [-5\sqrt{\varepsilon}, 5\sqrt{\varepsilon}] \times [-1 - 10\sqrt{\varepsilon}, -1 + 10\sqrt{\varepsilon}] \times [-10\sqrt{\varepsilon}, 10\sqrt{\varepsilon}]$. For simplicity, we choose the uniform mesh size $h = h_x = h_y = h_\xi = h_\eta$ and the time step $\tau = \frac{h}{4}$.

Example 4.2. The propagation equations of the Wigner measures corresponding to the solution to the Schrödinger equations (32) with the linear $E \otimes e$ Jahn–Teller potential V_{JT} can be written as the following Liouville equations:

$$\frac{\partial u_1}{\partial t} + \xi \frac{\partial u_1}{\partial x} + \eta \frac{\partial u_1}{\partial y} - \left(2x + \frac{x}{\sqrt{x^2+y^2}}\right) \frac{\partial u_1}{\partial \xi} - \left(2y + \frac{y}{\sqrt{x^2+y^2}}\right) \frac{\partial u_1}{\partial \eta} = 0, \tag{41}$$

$$\frac{\partial u_2}{\partial t} + \xi \frac{\partial u_2}{\partial x} + \eta \frac{\partial u_2}{\partial y} - \left(2x - \frac{x}{\sqrt{x^2+y^2}}\right) \frac{\partial u_2}{\partial \xi} - \left(2y - \frac{y}{\sqrt{x^2+y^2}}\right) \frac{\partial u_2}{\partial \eta} = 0 \tag{42}$$

with the initial values of u_1 and u_2 chosen as (36)–(38). We test the convergence of the original Schrödinger equation (32) toward the Liouville equations (41), (42) by varying the semiclassical parameter as $\varepsilon = 10^{-2}, 10^{-3}, 10^{-4}$.

The computational domain for the Liouville equations (41), (42) is chosen to be $[x, y, \xi, \eta] = [-12\sqrt{\varepsilon}, 12\sqrt{\varepsilon}] \times [-6\sqrt{\varepsilon}, 6\sqrt{\varepsilon}] \times [-1-12\sqrt{\varepsilon}, -1+12\sqrt{\varepsilon}] \times [-12\sqrt{\varepsilon}, 12\sqrt{\varepsilon}]$. For simplicity, we choose the uniform mesh size $h = h_x = h_y = h_\xi = h_\eta$ and the time step $\tau = \frac{h}{8}$.

Let

$$E^\varepsilon(t) = |P^\varepsilon_{sch}(t) - P^\varepsilon_{liou}(t)|$$

denote the absolute error of the upper level population during the hopping process for every fixed ε. The comparison of the model errors at $t = t_f$ between the Liouville solver and the Schrödinger solver; i.e., $E^\varepsilon(t_f)$ was done in [29]. Figure 4.3 shows that when varying the semiclassical parameter as $\varepsilon = 0.01, 0.001, 0.0001$, the error of the upper energy level populations converge in the order of $O(\sqrt{\varepsilon})$.

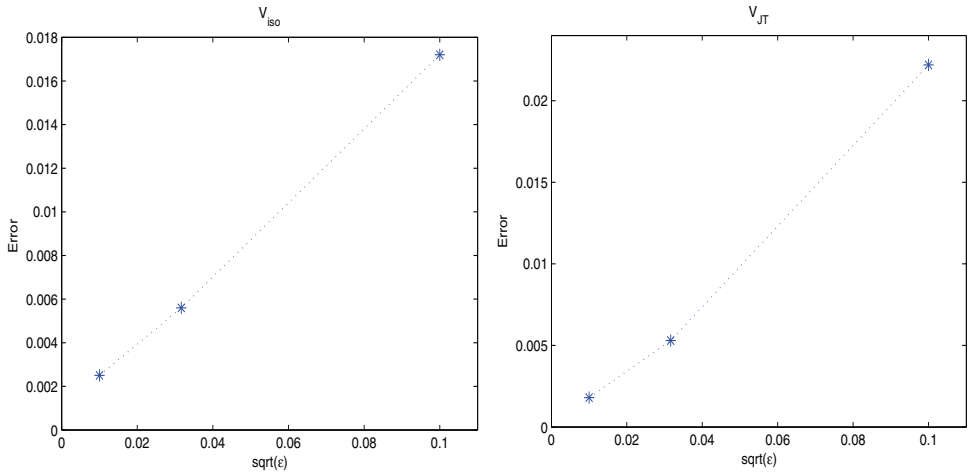

FIG. 4.3. *The error of the upper energy level populations as a function of* $\sqrt{\varepsilon}$ *when varying the semiclassical parameter* $\epsilon = 0.0001, 0.001, 0.01$. *The left is for the linear isotropic potential* V_{iso} *and the right is for the linear* $E \otimes e$ *Jahn–Teller potential* V_{JT}.

The probability density in the configuration space can be recovered by computing the zeroth moment,

$$(U_1)^n_{ij} = (U_1)(t^n, x_i, y_j) = \sum_{kl} (u_1)^n_{ijkl} h_\xi h_\eta.$$

For every fixed ε, we evaluate the accuracy of the high resolution finite volume scheme using the error of the population for the upper level defined by

$$E_{pop} = \sum_{i,j} U_{ij}^{num} h_x h_y - \sum_{i,j} U_{ij}^{exc} h_x h_y,$$

where the reference solution U^{exc} is approximated by the result obtained on a very fine mesh. We also use the l_1 norm error defined by

$$E_{l_1} = \sum_{i,j} |U_{ij}^{num} - U_{ij}^{exc}| h_x h_y.$$

Figures 4.4 and 4.5 show E_{pop} and E_{l_1} for the upper level probability density for the linear isotropic potential V_{iso} and the linear $E \otimes e$ Jahn–Teller potential V_{JT}, respectively, with different ε's. They are computed on different meshes in the phase space at $t = t_f$. One can see that solutions computed by our high resolution scheme converge in nearly second order to the reference solution, which is obtained using a very fine mesh. Since both potentials have similar conical crossings, our Eulerian surface hopping method has similar performances.

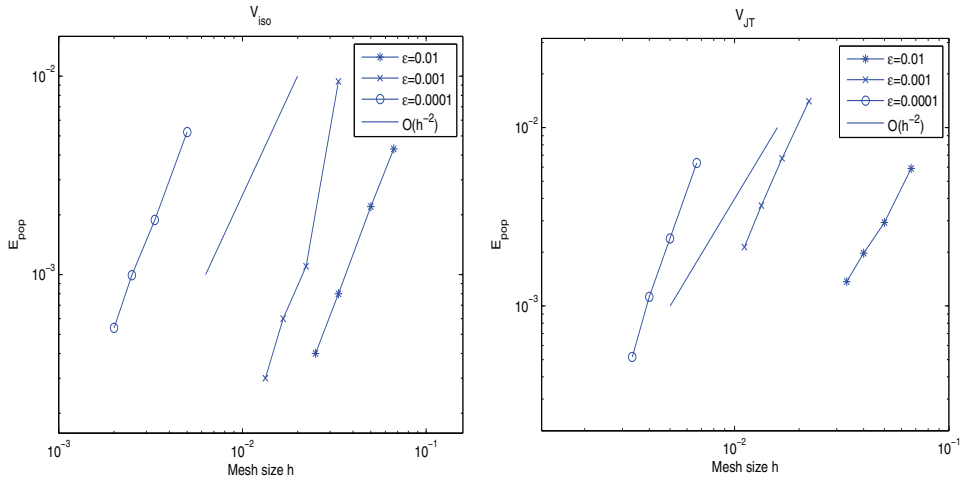

FIG. 4.4. *E_{pop}'s for different ε's. The left is for the linear isotropic potential V_{iso}, and the right is for the linear $E \otimes e$ Jahn–Teller potential V_{JT}.*

Figure 4.6 plots the evolution of the upper energy level population obtained by different schemes and meshes for the potential V_{iso}. One can see that compared with the second order scheme, the first order one is very diffusive even on a very fine mesh. The second order one gives better agreements with the "exact" solution obtained by the Schrödinger solver. After the hopping process, i.e., after time $t = 0.5$, the offset is due to the model error. For the potential V_{JT}, the result is similar and is omitted here.

Figure 4.7 shows the long time performance of our surface hopping method with V_{iso}. From time $t = 0.3$ to $t = 0.55$, it undergoes the first hopping process. Between the first ($t = 0.55$) and second ($t = 2.8$) hoppings the particles on the upper level will move in the original directions and the velocities will decrease, until the velocities become zero. Then they will turn back and accelerate toward the crossing point again.

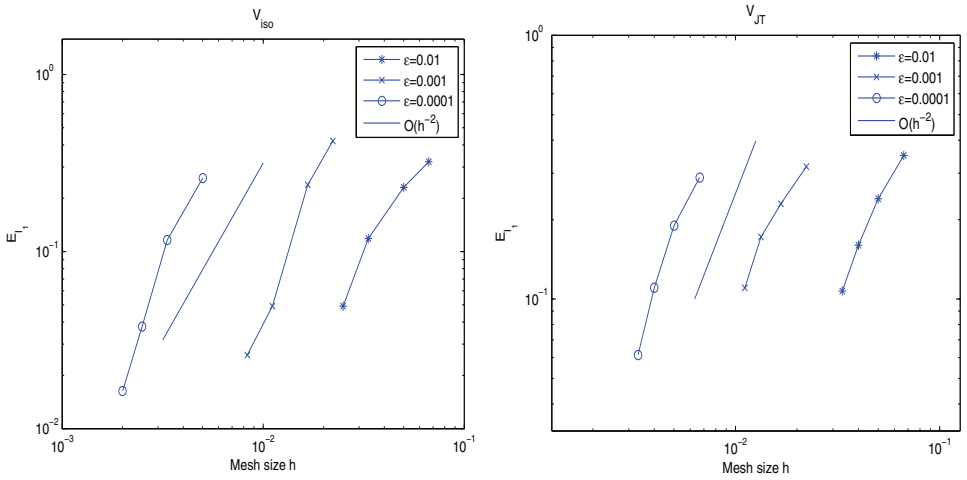

FIG. 4.5. *E_{l1} for different $\epsilon's$. The left is for the linear isotropic potential V_{iso} and the right is for the linear $E \otimes e$ Jahn–Teller potential V_{JT}.*

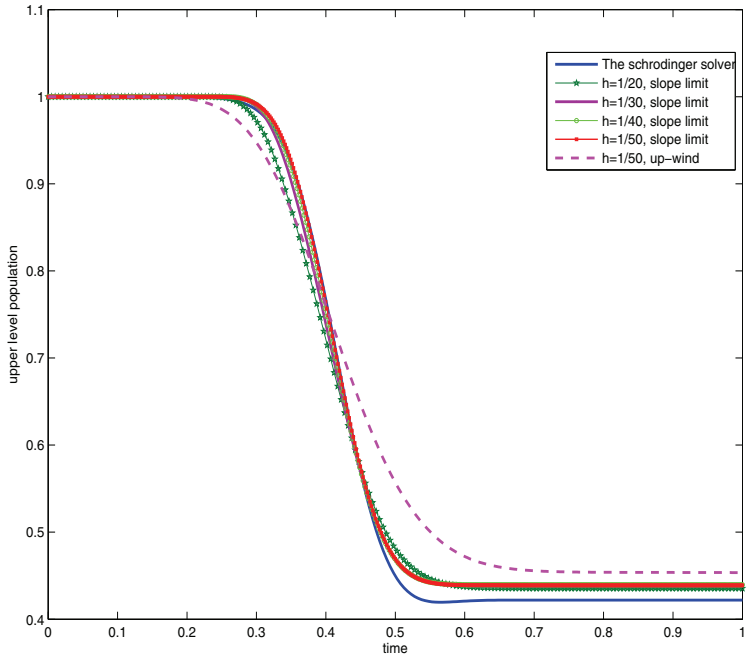

FIG. 4.6. *The comparison of different schemes and mesh sizes. The population of the upper energy level versus time are plotted. $\varepsilon = 0.01$.*

The second hopping process takes place between $t = 2.8$ and $t = 3.5$. One can see that our semiclassical method captures the population density quite accurately after the hoppings even by using a very coarse mesh.

Figure 4.8 gives a similar result as Figure 4.7, except that the potential V_{JT} is very steep so that three hopping processes occur during this time interval.

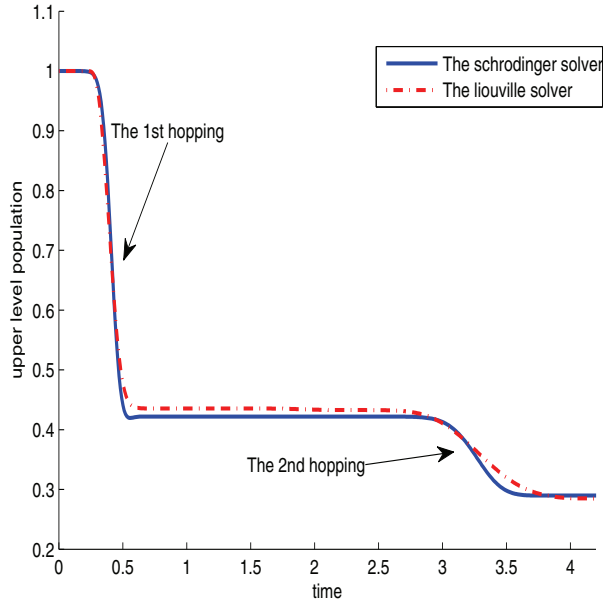

FIG. 4.7. *The long time behavior of the surface hopping process with the potential* V_{iso}. *The plot shows the population of the upper energy level versus time. The solid line corresponds to the Schrödinger solver and the dashed line corresponds to the Liouville solver.* $h = \frac{1}{20}$, $\Delta t = \frac{1}{100}$, *and* $\varepsilon = 0.01$.

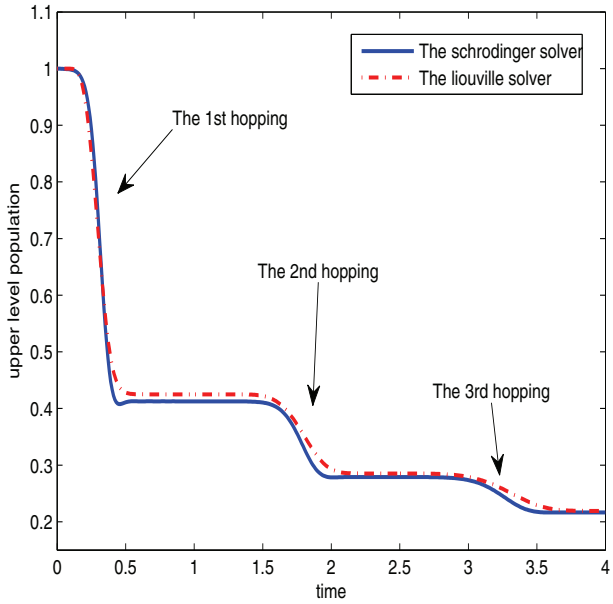

FIG. 4.8. *The long time behavior of the surface hopping process with the potential* V_{JT}. *The plot shows the population of the upper energy level versus time. The solid line corresponds to the Schrödinger solver, and the dashed line corresponds to the Liouville solver.* $h = \frac{1}{20}$, $\Delta t = \frac{1}{100}$, *and* $\epsilon = 0.01$.

5. Conclusion. In this paper, we constructed a surface hopping method for the Schrödinger equation with conical crossings in the *Eulerian* formulation. The method is based on the semiclassical approximation governed by the Liouville equations, which are valid away from the conical crossing manifold. At the crossing manifold, electrons hop to the other energy level with the probability determined by the Landau–Zener formula. This hopping mechanics is formulated as an interface condition, which is then built into the numerical flux for solving the underlying Liouville equation for each energy level. We studied the positivity, l_1 stability of the first order scheme, and conducted numerical experiments to study the accuracy and convergence rate of the proposed scheme. We also tested the long time behavior of the surface hopping process.

Constrained by the validity of the Landau–Zener formula, this algorithm cannot resolve the possible interferences between parts of the wave function originating from different levels. Such interferences might occur if classical trajectories on the upper and the lower energy levels arrive to the same point in the crossing set at the same time. Recently, Jin and Novak developed a coherent semiclassical transport model for pure-state quantum scattering problem using a complex Liouville equation, which retains the phase information needed for interference; see [17]. This idea could be combined with the approach of the current paper to deal with the interference at the hopping manifold, which will be studied in our future work.

6. Appendix: The Schrödinger solver. The reference solver for Schrödinger equation (32) is the operator splitting spectral method (refer to [28]). Consider the numerical solution on the bounded computational domain $D = [a_1, a_2] \times [b_1, b_2] \times [t_i, t_f]$. We divide the domain D by a set of lines parallel to the $x-, y-$ and t-axis to form a grid, and write $h_x = \frac{a_2-a_1}{I}$, $h_y = \frac{b_2-b_1}{J}$, and $\tau = \frac{t_f-t_i}{N}$ for the line spacings, where I, J, and N are three positive integers. For simplicity, we assume $h = h_x = h_y$. The crossing points Ω are set to be the grid points,

$$\Omega = \{(x_i, y_j, t_n) | x_i = a_1 + ih, y_j = b_1 + jh, t_n = n\tau, i = 0, ..., I, j = 0, ..., J, n = 0, ..., N\}.$$

Suppose $\Psi_{ij}^n = \{(\psi_{ij}^{n1}, \psi_{ij}^{n2})^T | 0 \le i \le I,\ 0 \le j \le J,\ 0 \le n \le N\}$ is the numerical solution on Ω, where Ψ_{ij}^n represents the approximation solution of wave function $\psi^\varepsilon(t, x, y)$ on the grid point (x_i, y_j, t_n).

From time $t = t_n$ to time $t = t_{n+1}$, where $t_{n+1} = t_n + \tau$, $t_0 = 0$, the numerical solution can be approximated by

$$\Psi_{ij}^{n+1} \approx \exp\left(\frac{i\epsilon\tau}{2}\Delta_{\mathbf{x}}\right) \exp\left(-\frac{i\tau}{\varepsilon}V(\mathbf{x})\right) \exp\left(\frac{i\varepsilon\tau}{2}\Delta_{\mathbf{x}}\right) \Psi_{ij}^n, \quad \mathbf{x} = (x, y).$$

The Laplace operator $\frac{i\epsilon\tau}{2}\Delta_{\mathbf{x}}$ can be efficiently approximated by the 2D fast Fourier transform algorithm. For the linear isotropic potential,

$$V_{iso}(\mathbf{x}) = \begin{pmatrix} x & y \\ y & -x \end{pmatrix}, \quad \mathbf{x} = (x, y) \in \mathbb{R}^2,$$

the operator $\exp(-\frac{i\tau}{\epsilon}V(\mathbf{x}))$ can be written as

$$\exp(-\frac{\tau}{\varepsilon}V_{iso}(\mathbf{x})) = \cos(\frac{\tau}{\varepsilon}|\mathbf{x}|)I - \frac{i}{|\mathbf{x}|}\sin(\frac{\tau}{\varepsilon}|\mathbf{x}|)V_{iso}(\mathbf{x}).$$

The linear $E \otimes e$ Jahn–Teller potential V_{JT} can be handled in the same way. In [2, 29], the authors proved the meshing strategy $h = O(\varepsilon)$, $\tau = o(\varepsilon)$ giving the l^2-approximation of the wave function, indicating that the operator splitting spectral

method can use mesh sizes much larger then finite difference methods. However when the semiclassical parameter ε is very small, the operator splitting spectral method is still very expensive.

Acknowledgments. Our understanding of the Born–Oppenheimer approximation and the surface hopping mechanism has benefited from the conversations with Victor Batista, Caroline Lasser, J.R. Schmidt, and Haobin Wang. We also appreciate the valuable discussions with Dongming Wei and Xu Yang. Zhiwen Zhang also thanks the financial support from the China Scholarship Council and the warm hospitality of Prof. Jin during his visit to the University of Wisconsin-Madison.

REFERENCES

[1] M. Baer and R. Englman, *A study of the diabatic electronic representation within the Born-Oppenheimer approximation*, Mol. Phys., 75 (1992), pp. 293–303.
[2] W. Bao, S. Jin, and P. Markowich, *On the time-splitting spectral approximations for the Schrödinger equation in the semiclassical regime*, J. Comput. Phys., 175 (2002), pp. 487–524.
[3] M. Born and R. Oppenheimer, *Zur Quantentheorie der Molekeln*, Ann. Phys., 84 (1927), pp. 457–484.
[4] L. J. Butler, *Chemical reaction dynamics beyond the Born-Oppenheimer approximation*, Annu. Rev. Phys. Chem., 49 (1998), pp. 125–171.
[5] J.-M. Combes, P. Duclos, and R. Seiler, *The Born-Oppenheimer approximation*, in Rigorous Atomic and Molecular Physics, G. Velo and A. Wightman, eds., Plenum Press, New York, 1981, pp. 185–212.
[6] K. Drukker, *Basics of surface hopping in mixed quantum/classical simulations*, J. Comput. Phys., 153 (1999), pp. 225–272.
[7] G. Folland, *Harmonic Analysis in Phase Space*, Ann. of Math. Stud. 122, Princeton University Press, Princeton, NJ, 1989.
[8] P. Gérard, P. A. Markowich, N. J. Mauser, and F. Poupaud, *Homogenization limits and Wigner transforms*, Comm. Pure Appl. Math., 50 (1997), pp. 323–379.
[9] G. Hagedorn, *A time dependent Born-Oppenheimer approximation*, Comm. Math. Phys., 77 (1980), pp. 1–19.
[10] G. Hagedorn, *High order corrections to the time-independent Born-Oppenheimer approximation I: Smooth potentials*, Ann. Inst. H. Poincaré Sect. A, 47 (1987), pp. 1–19.
[11] G. Hagedorn, *Molecular Propagation through Electron Energy Level Crossings*, Mem. Amer. Math. Soc. 111, American Mathematical Society, Providence, RI, 1994.
[12] G. A. Hagedorn and A. Joye, *A time-dependent Born-Oppenheimer approximation with exponentially small error estimates*, Comm. Math. Phys., 223 (2001), pp. 583–626.
[13] E. J. Heller, *Frozen Gaussians: A very simple semiclassical approximation*, J. Chem. Phys., 75 (1981), pp. 2923–2931.
[14] I. Horenko, C. Salzmann, B. Schmidt, and C. Schütte, *Quantum-classical Liouville approach to molecular dynamics: Surface hopping Gaussian phase-space packets*, J. Chem. Phys., 117 (2002), pp. 11075–11088.
[15] S. Jin and X. Liao, *A Hamiltonian-preserving scheme for high frequency elastic waves inheterogeneous media*, J. Hyperbolic Differ. Equ., 3 (2006), pp. 741–777.
[16] S. Jin and L. Novak, *A semiclassical transport model for thin quantum barriers*, Multiscale Model Simul., 5 (2006), pp. 1063–1086.
[17] S. Jin and K. Novak, *A coherent semiclassical transport model for pure-state quantum scattering*, Commun. Math. Sci., 8 (2010), pp. 253–275.
[18] S. Jin and D. Yin, *Computation of high frequency wave diffraction by a half plane via the Liouville equation and geometric theory of diffraction*, Commun. Comput. Phys., 4 (2008), pp. 1106–1128.
[19] S. Jin and X. Wen, *A Hamiltonian-preserving scheme for the Liouville equation of geometrical optics with transmissions and reflections*, SIAM J. Numer. Anal., 44 (2006), pp. 1801–1828.
[20] S. Jin and X. Wen, *Hamiltonian-preserving schemes for the Liouville equation with discontinuous potentials*, Commun. Math. Sci., 3 (2005), pp. 285–315.
[21] S. Jin and X. Wen, *Computation of transmissions and reflections in geometrical optics via the reduced Liouville equation*, Wave Motion, 43 (2006), pp. 667–688.

[22] C. F. Kammerer and C. Lasser, *Wigner measures and codimension two crossings*, J. Math. Phys., 44 (2003), pp. 507–527.
[23] C. F. Kammerer and C. Lasser, *Single switch surface hopping for molecular dynamics with transitions*, J. Chem. Phys., 128 (2008), pp. 5–9.
[24] M. Klein, A. Martinez, R. Seiler, and X. P. Wang, *On the Born-Oppenheimer expansion for polyatomic molecules*, Comm. Math. Phys., 143 (1992), pp. 607–639.
[25] S. Kube, C. Lasser, and M. Weber, *Monte Carlo sampling of Wigner functions and surface hopping quantum dynamics*, J. Comput. Phys., 228 (2009), pp. 1947–1962.
[26] L. Landau, *Zur theorie der Energieubertragung*, II. Phys. of the Soviet Union, 2 (1932), pp. 46–51.
[27] D. Landau and E. M. Lifschitz, *Quantum Mechanics: Non-Relativistic Theory*, 3rd ed., Pergamon Press, Oxford, 1977.
[28] C. Lasser, *Conical Energy Level Crossings in Molecular Dynamics*, Doctoral dissertation, Technische Universitt München, Germany, 2004.
[29] C. Lasser, T. Swart, and S. Teufel, *Construction and validation of a rigorous surface hopping algorithm for conical crossings*, Commun. Math. Sci., 5 (2007), pp. 789–814.
[30] C. Lasser and S. Teufel, *Propagation through conical crossings: An asymptotic semigroup*, Comm. Pure Appl. Math., 58 (2005), pp. 1188–1230.
[31] R. J. Leveque, *Finite Volume Methods for Hyperbolic Problems*, Cambridge University Press, Cambridge, 2002.
[32] P. L. Lions and T. Paul, *Sur les mesures de Wigner*, Rev. Mat. Iberoamericana, 9 (1993), pp. 553–618.
[33] D. Sholl and J. Tully, *A generalized surface hopping method*, J. Chem. Phys., 109 (1998), pp. 7702–7710.
[34] H. Spohn and S. Teufel, *Adiabatic decoupling and time-dependent Born-Oppenheimer theory*, Comm. Math. Phys. 224 (2001), pp. 113–132.
[35] S. Thiel, T. Kluner, and H. J. Freund, *Interference-effect in the laser-induced desorption of small molecules from surface: A model study*, Chem. Phys., 236 (1998), pp. 263–276.
[36] J. Tully and R. Preston, *Trajectory surface hopping approach to nonadiabatic molecular collisions: The reaction of H^+ with D_2*, J. Chem. Phys., 55 (1971), pp. 562–572.
[37] J. Tully, *Molecular dynamics with electronic transitions*, J. Chem. Phys., 93 (1990), pp. 1061–1071.
[38] A. Voronin, J. Marques, and A. Varandas, *Trajectory surface hopping study of the Li + Li_2 ($X^1\Sigma_g^+$) dissociation reaction*, J. Phys. Chem. A, 102 (1998), pp. 6057–6026.
[39] E. Wigner, *On the quantum correction for thermodynamic equilibrium*, Phys. Rev., 40 (1932), pp. 749–759.
[40] G. Worth and L. Cederbaum, *Beyond Born-Oppenheimer: Molecular dynamics through a conical intersection*, Annu. Rev. Phys. Chem., 55 (2004), pp. 127-158.
[41] C. Zener, *Non-adiabatic crossing of energy levels*, Proc. R. Soc. Lond. Ser. A Math. Phys. Eng. Sci., 137 (1932), pp. 692–702.